CHINESE OPTICS LETTERS

Vol. 21, No. 2 | February 2023

Laser frequency locking method for Rydberg atomic sensing

Kai Yang (杨 凯), Ruiqi Mao (毛瑞棋), Qiang An (安 强), Zhanshan Sun (孙占山)*, and Yunqi Fu (付云起)**

College of Electronic Science and Technology, National University of Defense Technology, Changsha 410073, China

*Corresponding author: szs199252@163.com

**Corresponding author: yunqifu@nudt.edu.cn

Received June 28, 2022 | Accepted September 8, 2022 | Posted Online November 14, 2022

Based on the Rydberg cascade electromagnetically induced transparency, we propose a simultaneous dual-wavelength locking method for Rydberg atomic sensing at room temperature. The simplified frequency-locking configuration uses only one signal generator and one electro-optic modulator, realizing real-time feedback for both lasers. We studied the effect of the different probe and coupling laser powers on the error signal. In addition, the Allan variance and a 10 kHz amplitude-modulated signal are introduced to evaluate the performance of the laser frequency stabilization. In principle, the laser frequency stabilization method presented here can be extended to any cascade Rydberg atomic system.

Keywords: Rydberg; electromagnetically induced transparency; laser frequency locking.

DOI: 10.3788/COL202321.021407

1. Introduction

In the past decade, Rydberg atomic electrometry has made substantial progress in the measurements of electromagnetic field amplitude[1–4], polarization[5], phase[6], and angle[7]. In these experiments, a weak probe laser excited the alkali metal atoms from their ground state to the intermediate state; meanwhile, an intense coupling laser excited the atoms from the intermediate state to a Rydberg state, forming an optical transmission window, which is known as electromagnetically induced transparency (EIT). The presence of an electromagnetic field will disrupt the EIT spectrum and change the optical transmission according to the AC Stark effect. When the frequencies of both the probe and coupling lasers are locked to the atomic transition, the electromagnetic field variation can be detected by the change of the probe laser transmission. Hence, the frequency stability of the probe and coupling lasers is a crucial technique for Rydberg atomic sensing, especially in the case of heterodyne scenarios[6–9].

In general, active laser frequency stabilization techniques can be roughly divided into two categories. One is locking the laser frequency to an external optical reference cavity, such as the Pound–Drever–Hall (PDH) method[10–14]. The other is using atomic transition spectroscopy for laser frequency stabilization, such as saturated absorption spectroscopy (SAS)[15], polarization spectroscopy[16], modulation transfer spectroscopy[17], and recently, EIT spectroscopy[18–20]. The cavity-locking methods are susceptible to environmental factors such as pressure and temperature and require additional means to shift the laser frequency to the atomic resonance transition, since the reference is the cavity rather than the atomic level. In contrast, the atomic transition spectral-locking methods can stabilize the laser frequency directly at the atomic resonance transition and are robust to external disturbances so that they can be one of the promising candidates for practical applications.

This work presents a simultaneous dual-wavelength locking method for Rydberg atom-based sensing by multiplexing the modulation signal. Based on the well-established modulated transfer spectroscopy technique, we extracted a portion of the modulated probe light that counterpropagates with an intense coupling light to generate the modulated EIT and the corresponding error signal. Then, we analyzed the variance of error signals under different probe and coupling laser powers. The Allan variance is introduced to evaluate the frequency stability of the coupling laser. Furthermore, the performance of our laser frequency stabilization technique was then assessed using a 10 kHz amplitude-modulated (AM) signal, which is one of the practical application scenarios for Rydberg atomic sensing. According to the ladder-type Rydberg EIT of cesium atoms, the probe laser is locked to the transition from the ground state ($6S_{1/2}$, $F = 4$) to the intermediate state ($6P_{3/2}$, $F' = 5$), while the coupling laser is locked to the transition from the intermediate state to the Rydberg state ($42D_{5/2}$). It should be noted that only one signal generator (SIG) and one electro-optic modulator (EOM) are required in the whole scheme. With merely an extra vapor cell and a lock-in amplifier, the frequency of the coupling laser can be easily locked to the excited-excited state transition.

This method can operate at room temperature and can endure minor mechanical jitter, making it more suitable for outdoor applications. In principle, the laser frequency locking technique can easily be extended to any cascade Rydberg atomic system.

2. Experimental Setup

The sketch of the experimental setup and the related three-level Rydberg ladder EIT are shown in Fig. 1. In Fig. 1(b), one can see that the 510 nm coupling laser is frequency-stabilized at the excited-excited state transition, i.e., the transition from the intermediate state ($|2\rangle$; $6P_{3/2}$, $F'=5$) to the Rydberg state ($|3\rangle$; $42D_{5/2}$). It requires an additional 852 nm probe laser to excite the atoms from the ground state ($|1\rangle$; $6S_{1/2}$, $F=4$) to the intermediate state. The probe laser is frequency-locked with a proven modulated transfer spectroscopy, as shown in Fig. 1(a)-I, while the coupling laser is frequency-locked using a modulated EIT signal, as shown in Fig. 1(a)-II.

In detail, the probe laser is frequency-modulated at $\omega_m/2\pi = 20$ kHz by an EOM (Thorlabs, EO-PM-NR-C1), which is driven by an amplified (Thorlabs, HVA200) sinusoidal signal from an SIG. The beam splitter (BS) divides the modulated probe light into two beams. One beam is used to produce the modulated transfer spectrum for probe laser frequency stabilization. To generate the modulated EIT spectrum, the other beam radiates into a 2.5 cm cesium cube before a density filter (DF), which is used to adjust the Rabi frequency of the probe light. In Zone II, this probe beam is counterpropagated and overlapped with an intense 510 nm coupling beam to reduce the Doppler broadening effect. The $1/e^2$ diameter of the probe light was approximately 678 μm, with power varying from 7.6 to 53.2 μW, while the coupling light had a $1/e^2$ diameter of about 885 μm and a power ranging from 3.6 to 91 mW. The modulated EIT signal is demodulated to produce the error signal in the lock-in amplifier, which is triggered by the exact SIG in Zone I. Subsequently, the frequency stability of the coupling light can be achieved by feeding back the error signal to the port of the piezoelectric ceramic transducer (PZT) voltage of the coupling laser, which has a response bandwidth from DC to 10 kHz.

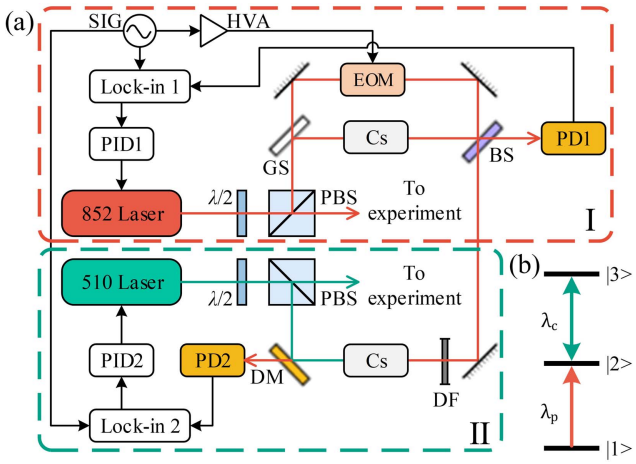

Fig. 1. Illustration of experimental scenarios and energy-level diagram. (a) Diagram of the experimental setup. Zone I is the scheme of the 852 nm probe laser frequency-locking process using the modulated transfer spectral signal. Zone II is the scheme of the 510 nm coupling laser frequency-locking process using the modulated Rydberg EIT signal. These two zones are connected by a typical frequency-modulated probe beam and a 20 kHz sinusoidal signal generated by the same SIG. λ/2, half-wave plate; PBS, polarizing beam splitter; GS, thick glass slide; BS, beam splitter; DF, density filter; DM, dichroic mirror; PD, photodetector; HVA, high-voltage amplifier. (b) Energy-level diagram of the Rydberg EIT ladder scheme consisting of the ground state $|1\rangle$ ($6S_{1/2}$, $F=4$), the intermediate state $|2\rangle$ ($6P_{3/2}$, $F'=5$), and the Rydberg state $|3\rangle$ ($42D_{5/2}$).

3. Results and Analysis

When the probe laser frequency is locked using the modulated transfer spectroscopy method, the Rydberg EIT spectrum and its corresponding error signal can be obtained by scanning the coupling laser frequency through the Rydberg transition $6P_{3/2}$, $F'=5 \rightarrow nD_{5/2}$ ($n=42$ in this work). Here, we studied the effects of both probe and coupling beam powers on the error signal, as shown in Fig. 2. By fixing the coupling beam power at 91 mW, we recorded the error signal at various probe beam powers of 8.2 μW (red curve), 32.1 μW (green curve), and 53.2 μW (blue curve), which is illustrated in Fig. 2(a). When the probe beam power is fixed at 7.6 μW, we got a couple of error signals shown in Fig. 2(b) by varying the coupling beam power at 3.6 mW (red curve), 18.1 mW (green curve), and 50.5 mW (blue curve),

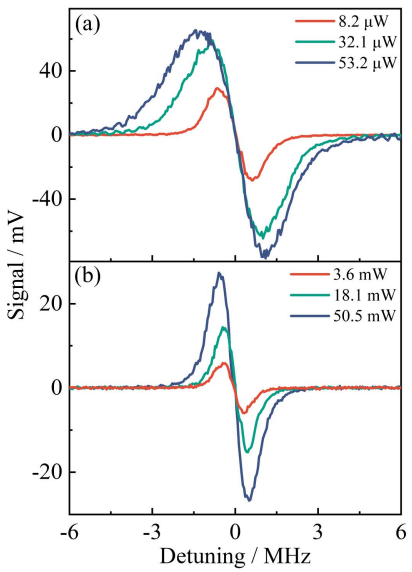

Fig. 2. Error signals under varying probe and coupling beam powers. (a) The coupling beam power is fixed at 91 mW, and the probe beam power is 8.2 μW (red curve), 32.1 μW (green curve), and 53.2 μW (blue curve), respectively. (b) The probe beam power is fixed at 7.6 μW, and the coupling beam power is 3.6 mW (red curve), 18.1 mW (green curve), and 50.5 mW (blue curve), respectively.

respectively. These figures clearly show that a more significant amplitude error signal can be obtained from a higher probe or coupling beam power, which is proportional to the amplitude of the EIT spectra. A larger error signal amplitude can make the frequency-locking system endure bigger frequency jitter during the stabilization process.

Moreover, the gradient of the error signal steepened with the increase of the coupling beam intensity at a fixed probe beam power. This can be attributed to the poor signal-to-noise ratio of the EIT spectrum at lower coupling beam power. A sharper error signal gradient guarantees a better frequency-stabilization performance, since the feedback loop gets more sensitive to frequency jitter. However, we found that the error signal shows negligible change when increasing the power of the coupling laser. Therefore, in the following experiments, the probe beam power is fixed at 32.1 μW, while the coupling beam power is set at 91 mW.

Figure 3 illustrates the frequency stability of the coupling laser with and without locking on for a given period of 500 s, which was monitored by a wavelength meter (Bristol Instruments, Model 671B). During the measurement under free-running conditions, the frequency of the coupling laser gradually shifted downwards over 800 MHz. After the proportional-integral-differential (PID) switch is locked on, the frequency stability of the coupling laser is significantly enhanced. The frequency fluctuation drops to ±11.2 MHz for a given 50 s monitoring period, and the corresponding root mean square (RMS) frequency jitter is 11.3 MHz over the entire 500 s measurement period. This frequency dither is much larger than that of Ref. [19], which is restricted by the measurement accuracy of the wavelength meter we used. It can be seen that the locked laser frequency still exhibits certain vibrations, which is due to the fact that the coupling laser is locked to the excited-excited state transition, and thus the frequency stabilization performance of the coupling laser is affected by the modulated transfer spectroscopy of probe light in addition to the modulated EIT method itself. Consequently, there are two kinds of factors for the instability: the transition between the ground state and the intermediate state and the transition between the intermediate state and the Rydberg state.

The figure of merit of frequency stabilization can be evaluated by the square root of the Allan variance, $\sigma(\tau)$[21], which is calculated as a function of the averaging time τ. With a measurement interval of 0.11 s, we recorded the $\sigma(\tau)$ of coupling laser frequency stabilization for both free-running (blue squares) and locking-on (red circles) conditions, as shown in Fig. 4. Here the results of error are demonstrated using double logarithmic coordinates in Fig. 4 for clarity, making it easier to graphically analyze the consequences of different types of noise. The dashed line represents the theoretical calculation curve, since the white noise and flicker phase noise for locking on are proportional to $\tau^{1/2}$. The minimum free-running $\sigma(\tau)$ is 7.64×10^{-9} at 0.88 s, and the minimum locking-on $\sigma(\tau)$ is 1.58×10^{-9} at 28.16 s. It can be observed that the $\sigma(\tau)$ in both cases basically overlapped with that of the theoretical curve within $\tau \sim 1$ s, indicating the dominant impact of white noise on the laser frequency-locking process. Then the free-running $\sigma(\tau)$ rises due to the accumulation of the PZT voltage dithering. In contrast, the locking-on $\sigma(\tau)$ still decreases according to the theoretical value until $\tau \sim 28$ s, which clearly proves that the laser frequency-locking method presented in this work can significantly improve the frequency stability.

Besides analyzing the square root of the Allan variance, we also use the AM signal to assess the efficacy of the frequency stabilization method in the context of Rydberg atom sensing. When the probe and the coupling lasers are simultaneously locked to the atomic transitions, the AM baseband signal can naturally be extracted in both resonant and off-resonant regions[22]. Specifically for the experiment, a 9.95 GHz RF signal with an AM frequency of 10 kHz and a modulation depth of 80% was irradiated into a cylindrical vapor cell with a length of 20 mm and a diameter of 10 mm. Here, in Fig. 5(a), it is obvious that the demodulated sinusoidal baseband signal has a period of

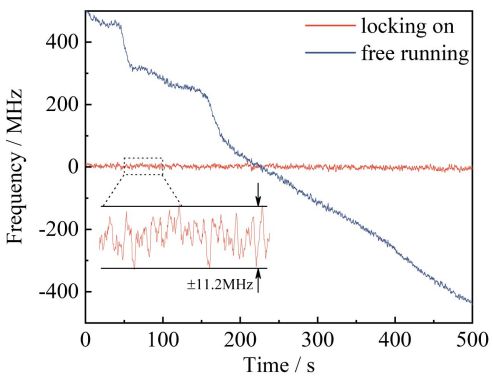

Fig. 3. Monitored laser frequency of the coupling laser with and without locking on for a given period of 500 s. After locking on, the coupling laser frequency stability is significantly improved. The inset is the zoom part of the dashed box, indicating that the corresponding frequency stability of the coupling laser reaches ±11.2 MHz for a specific period from 50 s to 100 s.

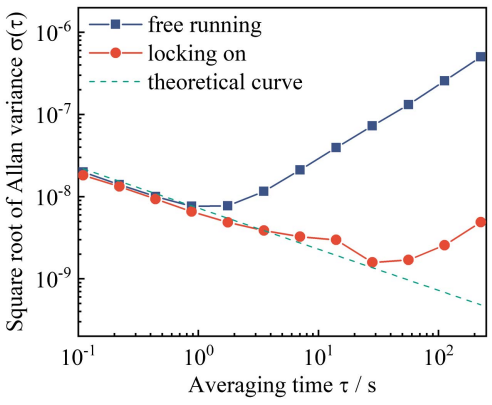

Fig. 4. The square root of Allan variance as a function of averaging time τ, under the coupling laser free-running (blue squares) and locking-on (red circles) conditions. The dashed line represents a theoretical curve with a slope of −0.5. The minimum measured $\sigma(\tau)$ with a measurement interval of 0.11 s is 7.64×10^{-9} in free-running condition and 1.58×10^{-9} in locking-on condition.

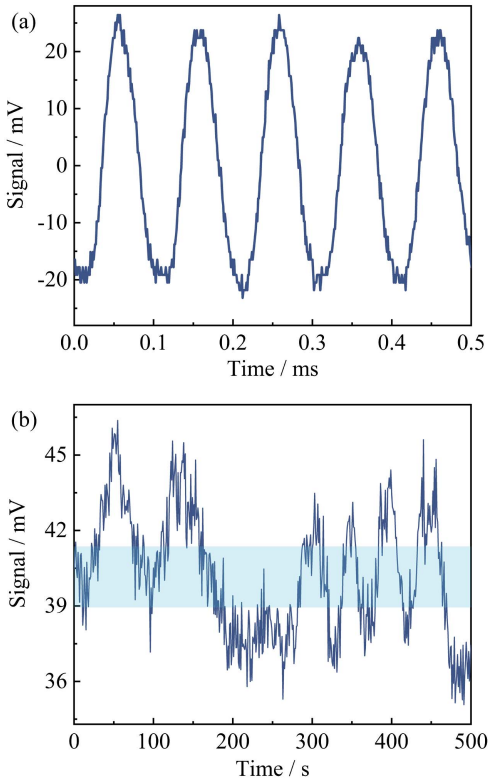

Fig. 5. The demodulated baseband signal and its corresponding peak-to-peak variation. (a) Demodulated signal with a modulation period of 0.1 ms; (b) monitored peak-to-peak values of the demodulated signal with a given measurement time of 500 s; the light blue area shows the standard deviation of the data.

0.1 ms, and the corresponding peak-to-peak value shows a little jitter over five cycles. Furthermore, we monitored the peak-to-peak variation over a given 500 s measurement time, as shown in Fig. 5(b). The peak-to-peak variation is roughly stable and varies from ~36 to ~45 mV, with a standard deviation of 2.4 mV. Note that the powers of both probe and coupling beams are not stabilized during the measurement, which has a slight effect on the peak-to-peak variation. In further detail, the laser power affects the height of the EIT, which in turn affects the response range of the Rydberg atoms to the intensity of the external electromagnetic field.

4. Conclusion

In summary, this work has demonstrated a simultaneous dual-wavelength locking technique for Rydberg atomic sensing. Based on a Rydberg cascade EIT, the probe laser frequency is locked at the transition from the ground state to the intermediate state using the modulated transfer spectroscopy method. To reduce the whole scheme's cost and complexity, we extract a fraction of the modulated probe laser from the modulated transfer spectroscopy zone to produce the modulated EIT spectrum. Subsequently, the error signal can be obtained by mixing the modulated EIT spectrum and the trigger signal, which is shared with the same SIG in the modulated transfer spectroscopy zone. In addition, the effect of the error signals under different probe and coupling beam powers is also studied. Lastly, the Allan variance and a 10 kHz AM signal are introduced to evaluate the performance of the coupling laser frequency stabilization, which proves the frequency-locking capacity of the simplified experimental strategy. In the future, we would take measures such as optimizing the PID parameters and eliminating the residual amplitude modulation in the EOM to further improve the frequency stability performance of the coupling laser. In general, the laser frequency-locking method presented here can extend to any cascade Rydberg atomic system. This approach is expected to apply to the Rydberg atom-based experiments, especially in outfield environments.

Acknowledgement

This work was supported by the National Natural Science Foundation of China (Nos. 61901495 and 12104509) and the Scientific Research Project of National University of Defense Technology (Nos. ZK19-20 and ZK20-13).

References

1. J. A. Sedlacek, A. Schwettmann, H. Kübler, R. Löw, T. Pfau, and J. P. Shaffer, "Microwave electrometry with Rydberg atoms in a vapour cell using bright atomic resonances," Nat. Phys. **8**, 819 (2012).
2. M. Y. Jing, Y. Hu, J. Ma, H. Zhang, L. J. Zhang, L. T. Xiao, and S. T. Jia, "Atomic superheterodyne receiver based on microwave-dressed Rydberg spectroscopy," Nat. Phys. **16**, 911 (2020).
3. C. L. Holloway, M. T. Simons, M. D. Kautz, A. H. Haddab, J. A. Gordon, and T. P. Crowley, "A quantum-based power standard: using Rydberg atoms for a SI-traceable radio-frequency power measurement technique in rectangular waveguides," Appl. Phys. Lett. **113**, 094101 (2018).
4. M. T. Simons, J. A. Gordon, C. L. Holloway, D. A. Anderson, S. A. Miller, and G. Raithel, "Using frequency detuning to improve the sensitivity of electric field measurements via electromagnetically induced transparency and Autler-Townes splitting in Rydberg atoms," Appl. Phys. Lett. **108**, 174101 (2016).
5. J. A. Sedlacek, A. Schwettmann, H. Kübler, and J. P. Shaffer, "Atom-based vector microwave electrometry using rubidium Rydberg atoms in a vapor cell," Phys. Rev. Lett. **111**, 063001 (2013).
6. M. T. Simons, A. H. Haddab, J. A. Gordon, and C. L. Holloway, "A Rydberg atom-based mixer: measuring the phase of a radio frequency wave," Appl. Phys. Lett. **114**, 114101 (2019).
7. A. K. Robinson, N. Prajapati, D. Senic, M. T. Simons, and C. L. Holloway, "Determining the angle-of-arrival of a radio-frequency source with a Rydberg atom-based sensor," Appl. Phys. Lett. **118**, 114001 (2021).
8. D. H. Meyer, P. D. Kunz, and K. C. Cox, "Waveguide-coupled Rydberg spectrum analyzer from 0 to 20 GHz," Phys. Rev. Applied **15**, 014053 (2021).
9. C. L. Holloway, M. T. Simons, J. A. Gordon, and D. Novotny, "Detecting and receiving phase-modulated signals with a Rydberg atom-based receiver," IEEE Antennas and Wireless Propag. Lett. **18**, 1853 (2019).
10. R. W. P. Drever, J. L. Hall, F. V. Kowalski, J. Hough, G. M. Ford, A. J. Munley, and H. Ward, "Laser phase and frequency stabilization using an optical resonator," Appl. Phys. B **31**, 97 (1983).
11. E. D. Black, "An introduction to Pound–Drever–Hall laser frequency stabilization," Am. J. Phys. **69**, 79 (2001).
12. S. Hirata, T. Akatsuka, Y. Ohtakem, and A. Morinaga, "Sub-hertz-linewidth diode laser stabilized to an ultralow-drift high-finesse optical cavity," Appl. Phys. Express **7**, 022705 (2014).

13. J. Sheng, Y. Chao, S. Kumar, H. Fan, J. Sedlacek, and J. P. Shaffer, "Intracavity Rydberg-atom electromagnetically induced transparency using a high-finesse optical cavity," Phys. Rev. A **96**, 033813 (2017).
14. H. M. Wang, Z. S. Xu, S. C. Ma, M. H. Cai, S. H. You, and H. P. Liu, "Artificial modulation-free Pound–Drever–Hall method for laser frequency stabilization," Opt. Lett. **44**, 5816 (2019).
15. D. A. Smith and I. G. Hughes, "The role of hyperfine pumping in multilevel systems exhibiting saturated absorption," Am. J. Phys. **72**, 631 (2004).
16. C. P. Pearman, C. S. Adams, S. G. Cox, P. F. Griffin, D. A. Smith, and I. G. Hughes, "Polarization spectroscopy of a closed atomic transition: applications to laser frequency locking," J. Phys. B **35**, 5141 (2002).
17. M. L. Harris, S. L. Cornish, A. Tripathi, and I. G. Hughes, "Optimization of sub-Doppler DAVLL on the rubidium D2 line," J. Phys. B **41**, 085401 (2008).
18. R. P. Abel, A. K. Mohapatra, M. G. Bason, J. D. Pritchard, K. J. Weatherill, U. Raitzsch, and C. S. Adams, "Laser frequency stabilization to excited state transitions using electromagnetically induced transparency in a cascade system," Appl. Phys. Lett. **94**, 071107 (2009).
19. Y. C. Jiao, J. K. Li, L. M. Wang, H. Zhang, L. J. Zhang, J. M. Zhao, and S. T. Jia, "Laser frequency locking based on Rydberg electromagnetically induced transparency," Chin. Phys. B **25**, 053201 (2016).
20. F. D. Jia, J. Zhang, L. Zhang, F. Wang, J. Mei, Y. H. Yu, Z. P. Zhong, and F. Xie, "Frequency stabilization method for transition to a Rydberg state using Zeeman modulation," Appl. Opt. **59**, 2108 (2020).
21. D. W. Allan, "Statistics of atomic frequency standards," Proc. IEEE Inst. Electr. Electron Eng. **54**, 221 (1966).
22. K. Yang, Z. S. Sun, R. Q. Mao, Y. Lin, Y. Liu, Q. An, and Y. Q. Fu, "Wideband Rydberg atom-based receiver for amplitude modulation radio frequency communication," Chin. Opt. Lett. **20**, 081203 (2022).